ELSEVIER

Computers and Geotechnics 23 (1998) 61–83

COMPUTERS AND GEOTECHNICS

# *H*-adaptive FE analysis of elasto-plastic non-homogeneous soil with large deformation

Y. Hu*, M.F. Randolph

*Special Research Centre for Offshore Foundation Systems, The University of Western Australia, Nedlands, WA 6907, Australia*

Received 16 December 1997; revised version recieved and accepted 15 June 1998

**Abstract**

Error estimation and *h*-adaptive finite element procedures are implemented for large deformation analyses of foundations on soil where the strength increases with depth. Errors are estimated by comparing strains at Gauss points with more accurate estimates using Superconvergent Patch Recovery (SPR). Mesh refinement using subdivision concept is then used iteratively to obtain optimal meshes, satisfying a minimum element size criterion. The Remeshing and Interpolation Technique with Small Strain (RITSS) approach is then used for large deformation analysis, with stress interpolation using either a modified form of the unique element method (MUEM), or the stress-SPR approach. Example analyses are then presented illustrating the three main aspects of mesh refinement, stress interpolation and large deformation response. Criteria are given for minimum element size and displacement increment for strip and circular foundations bearing on soil with varying degree of non-homogeneity, and computed bearing capacities are shown to compare well with lower bound estimates. The effect of soil weight on deep penetration of a strip foundation is discussed, with particular reference to the pattern of soil heave adjacent to the foundation, and the magnitude of the bearing capacity. 

## 1. Introduction

Finite element analysis has been used in engineering design for more than 20 years, but the accuracy of the analysis is still a major concern, particularly where non-linear material response occurs, or where large strains and deformations are involved. For such cases, it is also important to optimise the finite element mesh, taking due account of any non-homogeneity of material properties, in order to minimise computation times.

* Corresponding author.

0266-352X/98/$—see front matter 
PII: S0266-352X(98)00012-3

In offshore engineering, it is well known that the undrained shear strength $s_u$ of normally-consolidated (NC) or lightly over-consolidated (OC) marine clays increases more or less linearly with depth. This can be expressed as:

$$s_u = s_{uo} + kz \tag{1}$$

where $s_{uo}$ is the undrained shear strength at the clay surface and $k$ is the rate of increase in $s_u$ with depth $z$. For a foundation of width, $B$, the significance of the increase in strength with depth is generally indicated by the non-dimensional ratio, $kB/s_{uo}$. Typical values of $k$ will generally lie in the range of 0.6 to 3.0 kPa m$^{-1}$, while the surface strength, $s_{uo}$, may be as low as 10 to 20 kPa. As such, the non-homogeneity ratio $kB/s_{uo}$ may exceed 10 for foundations of 20 to 100 m in width. While for small values of $kB/s_{uo}$, it might be sufficiently accurate in practice to use average values of $s_u$ directly beneath the foundation, for larger values it is important to take account of the variation of $s_u$ with depth in bearing capacity calculations. It may also be pointed out that, for soft soils and large foundations, the magnitudes of settlement under working load conditions can be very large, and it is therefore necessary to make allowance for large strains and deformations in the numerical analysis.

The purpose of this paper is therefore twofold. It addresses the need to optimise finite element meshes in order to provide efficient but accurate computations, including a discussion of how non-homogeneity of the soil affects the choice of optimal mesh, and also shows how automatic optimal mesh generation, coupled with interpolation of all field quantities, provides a straightforward approach for problems involving large strains or deformations.

A numerical method for large deformation problems of soil has been developed by the authors [1], referred to as Remeshing and Interpolation Technique with Small Strain model (RITSS). This method has been used in pipeline and foundation penetration analyses [2–4]. Because the RITSS method is based on a standard small strain algorithm, but with frequent remeshing, it is very practical and easy to accommodate any complicated soil models. As such, it has a great potential to simulate a wide range of soil–structure interaction problems in offshore engineering. In previous work, the grading of each mesh was controlled using a simple exponential function with distance from a fixed origin. This did not give an optimal mesh in the calculation, and so accurate computations required very large numbers of elements. The purpose of this paper is to show how adaptive mesh generation techniques can be incorporated into the RITSS approach to provide accurate results, but with optimal meshes that minimise computational times.

Here, $h$-refinement will be used in the mesh generation and remeshing program. Because the soil is analysed as an elasto-plastic material, a strain error criterion is proposed, which is based on the superconvergent patch recovery (SPR) of strains. In the calculation of bearing capacity of strip foundations on non-homogeneous soil, an overriding (minimum) element size criterion and a displacement increment criterion are proposed, both of which are related to the soil rigidity index, $E/s_u$, and the degree of non-homogeneity, $kB/s_{uo}$. The FE numerical results have been

conducted with values of $kB/s_{uo}$ up to 30. Although most of the analyses have been conducted for strip foundations, application of the criteria to the bearing response of circular foundations on non-homogeneous soil is also illustrated. A more detailed study of circular foundations, using *h*-mesh refinement, will appear in a subsequent paper.

## 2. Mesh refinement in FE analysis

In finite element approximations, there are three common types of mesh refinement: *h*-refinement, *p*-refinement and *hp*-refinement. In *h*-refinement, the sizes, *h*, of the elements in high error regions are reduced; in *p*-refinement, the order, *p*, of the polynomial shape function is increased in specified elements; in *hp*-refinement, the element size, *h*, and the polynomial shape function of order, *p*, are adjusted simultaneously. In the present paper, *h*-refinement is adopted, as it is applicable to all existing codes. The process of *p*-refinement, in which the polynomial order of some elements is changed, requires new code development but can be very efficient especially if very high accuracy is desired and computing time are less important [5].

When *h*-refinement is employed, there are many ways to achieve an improved mesh. Mesh subdivision is probably the simplest of these, and has been used in early adaptive computations in which local mesh halving was used repeatedly. However, such processes are uneconomical and involve complex transitions. A better alternative is a complete mesh regeneration, which can be guided by specified mesh density requirements.

All adaptive FE analyses include three stages:

(a) obtain a solution with any existing mesh and estimate the error;
(b) predict the required refinement for achieving a specified accuracy;
(c) implement this refinement and develop a new mesh, and then obtain a new solution and estimate the new error.

Steps (b) and (c) are repeated until the required accuracy is achieved.

In effecting this process, it is essential to consider economy. In *h*-refinement, the aim is to generate a mesh with the smallest number of elements and to achieve the required accuracy at the same time. In this study, a refinement which combines subdivision and mesh regeneration is found to be very effective in producing a mesh of the required accuracy for elasto-plastic analysis.

### 2.1. Error estimation

In FE analysis the error is due to spatial discretization, but estimation of the error is not a simple task. Much research has been done in this area over the last decade. Belytschko and Tabbara [6] have studied four types of element error measures for dynamic problems with localization. They are (a) Zienkiewicz–Zhu criterion [7]; (b) Babuska–Rheinboldt criterion [8]; (c) Interpolation criterion [9]; and (d) Strain-projection criterion proposed by the authors [6]. It was found that the first three

criteria (a), (b) and (c), which work very efficiently for linear elastic problems, were not effective for localization problems. They failed to indicate the need for refinement in the area of localization, where the strain gradients are very large but the stress field is nearly uniform. The strain-projection criterion, which is based on an $L_2$-projection of strains, similar to the $L_2$-projection of stress [7,10] worked very well in capturing the area of localization.

Following the study by Belytschko and Tabbara [6], a strain-SPR criterion is proposed here,

$$\mathbf{e}_i^* = \left[ \left\{ \int_{\Omega_i} \left(\varepsilon^* - \varepsilon^h\right)^T \left(\varepsilon^* - \varepsilon^h\right) \mathrm{d}\Omega / \Omega_i \right]^{1/2} \right. \tag{2}$$

in which $\mathbf{e}_i^*$ is the strain error in element $i$, $\Omega_i$ is the area of element $i$ in two-dimensional analysis (or the volume of element $i$ in three-dimensional analysis), $\varepsilon^h$ are the strains from the FE solution, $\varepsilon^*$ is evaluated by SPR in a similar manner to the SPR of $\sigma^*$ by Zienkiewicz and Zhu [11]. This measure represents the strain error in an element and is convenient to use because it is non-dimensional.

### 2.2. Superconvergent patch recovery of strain

In error estimation, the essence of the procedure is to use the difference between the values of the post-processed, recovered, more accurate gradients (strain) $\varepsilon^*$ and those given directly by the FE solution $\varepsilon^h$. It is obvious that the success of the procedure is dependent on the accuracy of the recovered gradients. The global $L_2$-projection and simple averaging techniques were originally recommended by Zienkiewicz and Zhu [7], but it was soon found that such recovery techniques were inadequate for quadratic approximations, so that empirical correction factors were introduced early to increase the computed error values, which were always underestimated.

It is well known that the FE-solutions for $\sigma^h$ and $\varepsilon^h$ have a high quality at some special points, and these are referred to as superconvergent values [11]. Post-processing is aimed at fitting higher order local fields $\sigma^*$ and $\varepsilon^*$ to the superconvergent values,

$$\sigma_p^* = \mathbf{Pa} \left( \text{or } \varepsilon_p^* = \mathbf{Pa} \right) \tag{3}$$

where the subscript $p$ refers to the local patch, $\mathbf{P}$ contains appropriate polynomial terms and $\mathbf{a}$ is a set of unknown parameters.

In the present study, six-noded triangular elements, each containing three internal Gauss points, are used in a two dimensional (plane strain or axisymmetric) FE mesh. Thus, the quadratic terms for $\mathbf{P}$ and the six parameters in $\mathbf{a}$ are:

$$\mathbf{P} = \left[1, x, y, x^2, xy, y^2\right] \tag{4}$$

$$\mathbf{a} = [a_1, a_2, a_3, a_4, a_5, a_6]^T \tag{5}$$

The determination of the unknown parameters in **a** is best made by ensuring a least square fit of this to the set of superconvergent (or at least high accuracy) sampling points in the patch. This requires minimisation of

$$F(\mathbf{a}) = \sum_{i=1}^{n}\left(\varepsilon^h(x_i', y_i') - \varepsilon_p^*(x_i', y_i')\right)^2 = \sum_{i=1}^{n}\left(\varepsilon^h(x_i', y_i') - \mathbf{P}(x_i', y_i')\mathbf{a}\right)^2 \tag{6}$$

where $(x_i', y_i')$ are the normalised coordinates of a group of sampling points, $n = mk$ is the total number of sampling points, with $m$ being the number of elements in the patch (see Fig. 1) and $k$ the number of sampling points on each element.

It should be noticed that difficulties can be encountered when absolute values of coordinates $(x_i, y_i)$ are used, particularly for higher order elements that have a significant size as the equations become ill-conditioned [12]. To avoid this difficulty, normalised coordinates should be used in the procedure. For the two-dimensional element patch in Fig. 1, the coordinates can be normalised as:

$$x_i' = -1 + 2\frac{x_i - x_{\min}}{x_{\max} - x_{\min}} \tag{7}$$

$$y_i' = -1 + 2\frac{y_i - y_{\min}}{y_{\max} - y_{\min}} \tag{8}$$

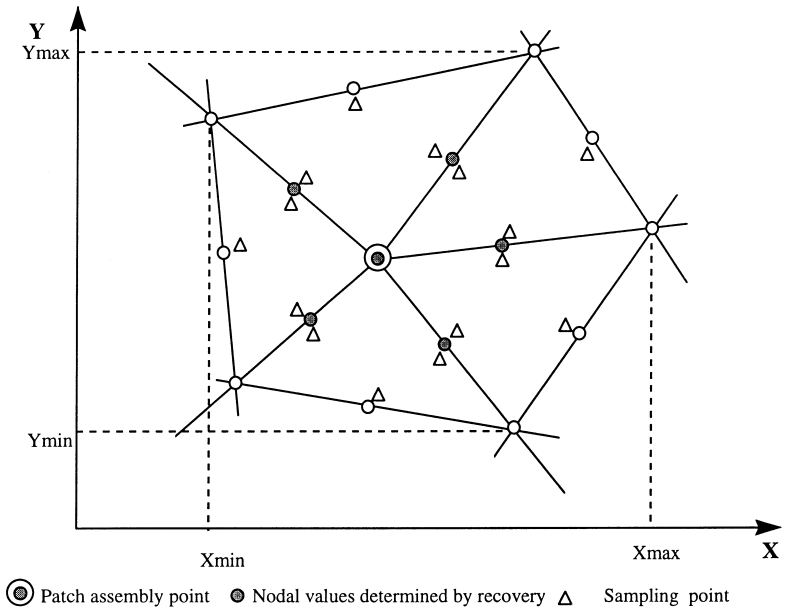


Fig. 1. A patch of quadratic triangular elements.

Here $x_{\max}$ and $x_{\min}$ denote the maximum and minimum values of the $x$-coordinates in the patch respectively, and similarly for $y_{\max}$ and $y_{\min}$ (see Fig. 1). Thus the range of the normalised variables is given by $-1 \le x'_i \le 1$ and $-1 \le y'_i \le 1$.

The minimisation condition of $F(\mathbf{a})$ implies that $\mathbf{a}$ satisfies

$$\sum_{i=1}^{n} \mathbf{P}^T(x'_i, y'_i)\mathbf{P}(x'_i, y'_i)\mathbf{a} = \sum_{i=1}^{n} \mathbf{P}^T(x'_i, y'_i)\varepsilon^h(x'_i, y'_i) \tag{9}$$

This can be solved in matrix form as

$$\mathbf{a} = \mathbf{A}^{-1}\mathbf{b} \tag{10}$$

where

$$\mathbf{A} = \sum_{i=1}^{n} \mathbf{P}^T(x'_i, y'_i)\mathbf{P}(x'_i, y'_i) \tag{11a}$$

and

$$\mathbf{b} = \sum_{i=1}^{n} \mathbf{P}^T(x'_i, y'_i)\varepsilon^h(x'_i, y'_i) \tag{11b}$$

The number of equations to be solved for each patch is modest and the recovery is performed only for each vertex node. Therefore the procedure is quite inexpensive.

Once parameters $\mathbf{a}$ are determined, the recovered nodal values of $\varepsilon^R$ are simply calculated by insertion of appropriate coordinates into the expression for $\varepsilon_p^*$ [Eq. (3)]. Here only the nodes inside of the patch are considered, as shown in Fig. 1. When the whole domain is recovered, the values of strains at any position can be calculated using

$$\varepsilon^* = \mathbf{N}\varepsilon^R \tag{12}$$

where $\mathbf{N}$ is the shape function for interpolation of displacements, and $\varepsilon^R$ are the recovered nodal strains. For some nodes in the mesh, the strains are recovered twice, and so the average values on these nodes are used.

For a patch of quadrilateral elements it is well known that the derivatives at appropriate Gauss points are superconvergent. However for a patch of triangular elements such as Fig. 1, the existence and the locations of superconvergent points are still a matter that does not appear to have been fully explored mathematically. It has been found experimentally that for quadratic (6-noded) triangles the central values at sides are optimal and the resulting recovered values at nodes are "ultra-convergent", i.e. with order of $O(h^4)$ [11]. Therefore, for the work reported here, the values of strains at each mid-side node have been obtained by interpolation (or extrapolation) of the three Gauss points in the element and these values are then used in the SPR procedure.

It can be noted that the sampling points used here do not coincide with the internal Gauss points. The reason for not using the mid-side sampling points as Gauss

points in the calculation is that the mid-side Gauss points are inferior to internal Gauss points for the six-noded triangular element, and also special treatment would be needed for the Gauss points along the centreline for axi-symmetric problems, where the radius is zero. Zienckwicz and Zhu [11] confirm that it is sufficient to use the mid-side points as sampling points (and not as Gauss points) in the SPR technique.

### 2.3. Adaptive strategies

In practical applications, an acceptable value of error must be specified in any given element, with the aim to reduce the error in each element to (or below) this value. Unfortunately in plastic analysis with localization problems the specification of maximum tolerance levels for the error measure **e*** is not easy. This is because there does not appear to exist a global error norm similar to the energy norm in self-joint elliptic problems due to the loss of elipticity. Therefore, a new error measure, a strain-SPR error criterion [Eq. (2)] is proposed, similar to the strain-projection error measure proposed by Belytschko and Tabbara [6]. In adaptive plastic analysis, researchers have tended to focus on capturing plastic local failure [13,14]. However, these methods are not suitable for the analysis of large deformation problems since continuous deformation needs to be simulated.

In problems that contain singularities, such as the sharp corner at the edge of a footing, adaptive mesh refinement does not necessarily lead to a reduction in the maximum error density, as defined by [Eq. (2)]. Instead, the region of significant error surrounding the singularity shrinks, and the total error (for a given energy input due to externally applied forces) reduces, but only at a slow rate. As such, it is necessary to stipulate a minimum element size, $h_{\min}$, rather than a target value of **e***.

This point is illustrated in Fig. 2, which shows contours of error density in the vicinity of the edge of a footing, as the mesh is gradually refined. It may be seen that the maximum energy density contour actually increases from 0.2 to 4 as the mesh is refined, but the area of significant error shrinks. The total (normalised) error $|\mathbf{e}|$, defined as:

$$| \mathbf{e} | = \frac{\sum_{i=1}^{n} \mathbf{e}_i * \Omega_i}{\sum_{i=1}^{n} | \varepsilon_i^h | \Omega_i} \tag{13}$$

and

$$| \varepsilon_i^h | = \left[ \left\{ \int_{\Omega_i} \left(\varepsilon^h\right)^T \left(\varepsilon^h\right) \mathrm{d}\Omega \right\} / \Omega_i \right]^{1/2} \tag{14}$$

reduces gradually from 34% to less than 15% (taking $h_{\min}$ as 1% of the footing width). Moreover the value of $|\mathbf{e}|$ also depends on displacement increment. Thus it cannot give a unique total error measure.

Using the strain-SPR error measure, the following refinement procedures are proposed in order to satisfy a specified minimum size of element ($h_{\min}$).

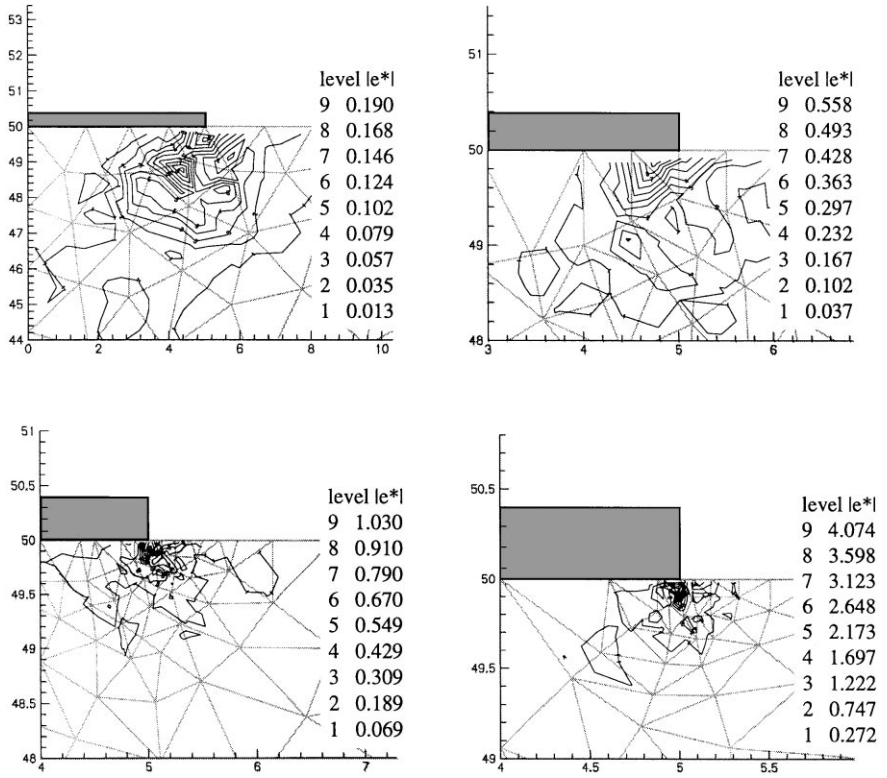


Fig. 2. Error density contours during mesh refinement.

*2.3.1. One-cycle mesh refinement*

In this refinement, when the minimum size of elements $h_{\min}$ is given, refinement will be accomplished in one cycle. The following steps are required:

Step 1. Build a coarse mesh; compute an initial solution.
Step 2. Calculate more accurate strain ε* using SPR.
Step 3. Estimate the error over the mesh using Eq. (2).
Step 4. Compute $\mathbf{e}^*_{\max}$, the maximum element error over the mesh.
Step 5. Reset the mesh densities for all elements $\lambda_i \geq 1.0$ [see Eq. (13)].
Step 6. Regenerate the mesh using the new mesh density field.

In step 5, when $h_{\min}$ is given, for an element $i$, a local refinement parameter $\lambda_i$ may be defined as

$$\lambda_i = \frac{e_i^*}{|\,\mathbf{e}_n\,|} \tag{15}$$

and

$$|\,\mathbf{e}_n\,| = \eta \cdot M \cdot \left\{ \left[ \sum_{i=1}^{n} \left( |\,\varepsilon_i^h\,| + |\,\mathbf{e}_i\,| \right) \right] / n \right\} \tag{16}$$

in which $|\mathbf{e}_n|$ is the permissible strain error in every element, where $\eta$ is a permissible coefficient and $M$ is a safety factor. In the present work, $\eta = 10\% = 0.1$ and $M = 0.8$ have been adopted. This procedure has been used successfully in elastic analysis where Eq. (16) can be seen as a strain error norm. However, in elastoplastic analysis, this can only be used for a guidance of the new element sizes because of the loss of elipticity in the plastic equations. The iterative approach for elastoplastic analysis is illustrated in Fig. 2, using Eqs. (13) and (14).

When $\lambda_i \geq 1.0$, the element $i$ needs to refined. The new element size for element $i$ is predicted as

$$h_{\text{new}} = \frac{h_{\text{exist}}}{\lambda_i^{1/p}} \tag{17}$$

in which $p$ is the polynomial order of the finite element space. In the neighbourhood of a singularity, $p$ is replaced by a parameter defining the strength of the singularity (generally $p = 0.5$ is used in this situation). For any element, if $h_{\text{new}} < h_{\min}$, $h_{\min}$ is used. When $\lambda_i < 1.0$, the element size may be increased without exceeding the error tolerance. However, since a coarse mesh was used to start with, further coarsening of the mesh is not normally carried out which is equivalent to taking $\lambda_i = 1$.

*2.3.2. Refinement using subdivision concept*

In this procedure, a few cycles may be needed before the minimum size of the elements in the mesh reaches the required $h_{min}$. However, multiple cycles are only performed before the start of the large deformation analysis, after which one cycle is inserted in each remeshing. The steps are:

Step 1. Build a coarse mesh; compute an initial solution.
Step 2. Calculate the recovered, more accurate strain ε* using SPR.
Step 3. Estimate the strain error over the mesh using Eq. (2).
Step 4. Compute $\mathbf{e}^*_{max}$, the maximum element error over the mesh.
Step 5. Reduce the element sizes by a factor of 2 for all elements in which $\mathbf{e}^*_i \geq \theta \mathbf{e}^*_{\max}$, where $0 \leq \theta \leq 1$.
Step 6. Regenerate the mesh using the updated mesh density.
Step 7. Check if the minimum element size in the new mesh $\leq h_{\min}$; if not, compute the new solution and go to Step 2; otherwise stop.

In Step 5, $\theta$ has been chosen as 0.5, as suggested by Mucke and Whiteman [15] in subdivision mesh refinement. They concluded that in the range $0.3 \leq \theta \leq 0.8$ the mesh sequences and the convergence order were similar.

## 3. Interpolation method

In large deformation analysis using RITSS [1], stresses and soil properties have to be interpolated from the old mesh to the new mesh after each remeshing. The interpolation method that was found to work best was the unique element method

(UEM), where the variables are interpolated entirely according to which element of the old mesh contains the new field points. This method was proposed on the basis of the stress field characteristics in a six-noded triangular element mesh, where the stresses vary linearly within each element but are discontinuous between adjacent elements. The procedure of the UEM is explained briefly by the following steps.

(a) Update the coordinates of the old mesh (according to displacements over the previous solution steps) to form a reference mesh;
(b) Find which element of the reference mesh contains the particular Gauss point of the new mesh;
(c) Interpolate (or extrapolate) the stress values at the new Gauss point using the three Gauss points in the reference element.

Difficulty has been encountered when this UEM is used in stress interpolation, owing to poor accuracy of the interpolated stress field at the edges of elements in the reference mesh. Fig. 3 shows an element in the reference field. A, B, C are three vertices and **a**, **b**, **c** are three Gauss points. If the new Gauss point lies in $\Delta$abc, like point $G_1$, the stress values can be interpolated very well. However, if the new Gauss point lies in $\Delta$ABC but outside of $\Delta$abc the extrapolated stress values for the new Gauss point may be very inaccurate, especially when the stress gradients are large. To overcome this, stress values at the sides of original triangle, $\Delta$ABC, like point $G_2$, are estimated using a linear interpolation between the closest point on **ab** and the corresponding point in the adjacent triangle $\Delta$ABD. Stress values for Gauss points that fall near the vertices of $\Delta$ABC, within the shaded areas shown in Fig. 3, such as point $G_3$, are merely assigned the same value of stress as point **b**. More importantly the yield status is checked after interpolation, which means if any new Gauss point that lies in the yielded zone of the reference field should stay on the yield surface.

The other interpolation method that is tested here is using the stress field obtained from a stress-SPR approach. In this method, the stress field from the FE solution is smoothed by the SPR, to give unique nodal stress values. Then the shape function $N$ for displacement in the mesh is used to interpolate stress values at the new Gauss

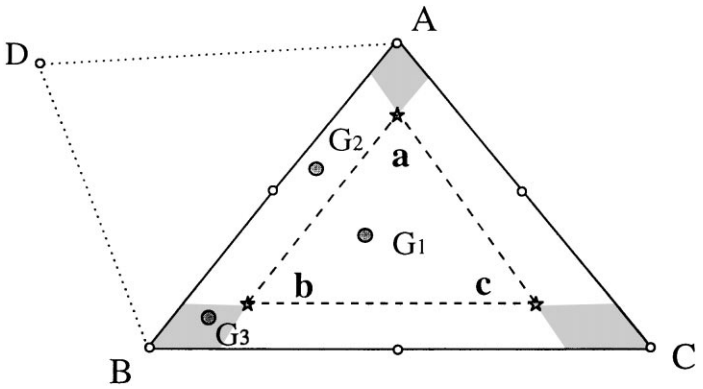


Fig. 3. An element in reference mesh for stress interpolation.

points [like Eq. (12), but for stress $\sigma$ instead of strain $\varepsilon$]. Again, the yielded status is checked for each new Gauss point.

In both the MUEM and SPR approaches, it was found to be critical to ensure that the stress field within a region that is at yield before remeshing stays on the yield surface in the interpolated stress field.

## 4. Numerical analyses and results

In all the following finite element simulations, the small strain analysis has been implemented by the AFENA finite element package, which was developed at the Centre for Geotechnical Research, University of Sydney [16]. In AFENA, a non-linear analysis is conducted without iteration. After any increment, if the stresses on a Gauss point go outside the yield surface, they will be corrected back to the yield surface. The out-of-balance force generated by this correction will be carried into the next incremental calculation. Therefore all the criteria for element size and displacement increment size introduced below must be viewed in relation to this solution algorithm. In all analyses, six-noded triangular elements containing three Gauss points are used.

In all the following analyses, soil is considered as an elastic perfectly-plastic material with Von Mises yield criterion. An associated flow rule is adopted, with undrained conditions assumed. Soil properties have been chosen as $E/s_u = 500$ (where $E$ is Young's modulus and $s_u$ is the undrained shear strength), Poisson's ratio, $\nu = 0.49$, and friction and dilation angles $\phi = \psi = 0$. Soil self-weight is not considered in bearing capacity analysis (with no remeshing) since it is not relevant; it is only considered in penetration analysis (large deformations, with remeshing).

### 4.1. Interpolation techniques

The two interpolation techniques for the stress field tested here are MUEM and SPR. To illustrate the computed responses using these two interpolation techniques, a rigid rough strip footing penetrating into homogeneous soil has been analysed.

In these analyses, the soil semi-field is taken as 7 times the semi-width of the footing in width, and 4 times the footing semi-width in depth. A relatively coarse mesh (Fig. 4) was used for the interpolation testing, since the primary concern was to assess the smoothness of the computed load–displacement response, rather than the absolute accuracy. Displacement increment and remeshing interval were taken as $\delta(v/B) = 0.002$ and $\Delta(v/B) = 10 * \delta(v/B) = 0.02$, where $v$ is the vertical displacement of the foundation.

Hu and Randolph [1] showed that the UEM interpolation technique worked well for the overall load–displacement response. However, after each interpolation a small fluctuation appeared in the load–displacement response [Fig. 5(a)]. The MUEM approach gave smaller fluctuations, while "saw-tooth" were noted using the SPR approach, but without correcting of the stress field back on to the yield envelope where appropriate. However, when this correction is made, both the modified

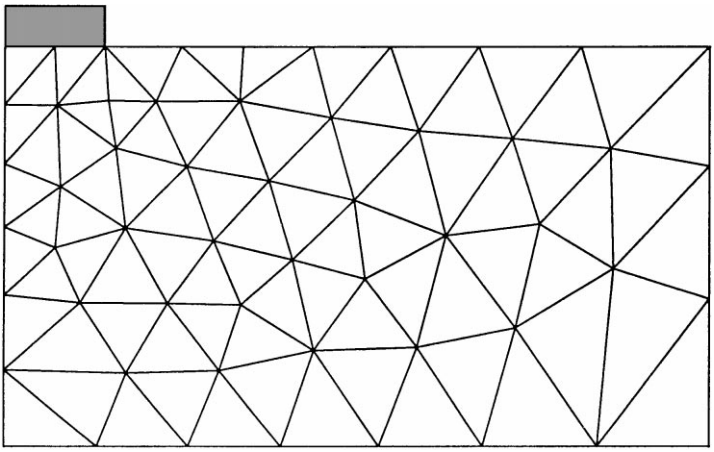

Fig. 4. Mesh for testing interpolation technique.

(MUEM) unique element method and the SPR approach give a smooth load–displacement response, with excellent agreement between the two approaches [Fig. 5(b)]. The computed response without remeshing is also shown for comparison. This lies beneath the other two responses, because no allowance is incorporated for the increasing penetration of the footing. Note that all three analyses overpredict the true bearing capacity ($q_u/s_u = 5.14$) because of the rather coarse mesh used. It should be pointed out that the meshes used in the analyses (indicated in the legends of Fig. 5) are initial meshes before any remeshing.

### 4.2. H-Adaptive mesh generation methods

To test the two adaptive refinements introduced in the section "Adaptive strategies" above, a rough strip foundation on homogeneous soil is analysed. The initial coarse mesh is shown in Fig. 6, in which the discretised (semi) domain extends to 10 times the semi-width of the footing, both laterally and vertically.

Fig. 7 shows the meshes using the two different adaptive strategies and also an exponential density function centred on the edge of the footing. In all cases, the same minimum element size tolerance is used, with $h_{min} = 1\% * B = 0.1$ m. The mesh in Fig. 7(a) was generated in a single cycle (section "One-cycle mesh refinement" above), while that in Fig. 7(b) was generated after three adaptive cycles of halving element sizes in regions of high error density (section "Refinement using subdivision concept", above). The numbers of elements (NUMEL) in meshes (a), (b) and (c) are 352, 209 and 1166, respectively.

The computed normalised bearing capacities ($q_u/s_{uo}$) for the three cases were 5.33, 5.34 and 5.30 (3.7, 3.9 and 3.1% above the analytical solution of 5.14) using meshes 7(a), 7(b) and 7(c), respectively. It is apparent that although mesh 7(c) gives slightly higher accuracy, the high number of elements would be very expensive computationally. The optimum approach seems to be the "element subdivision" approach of the

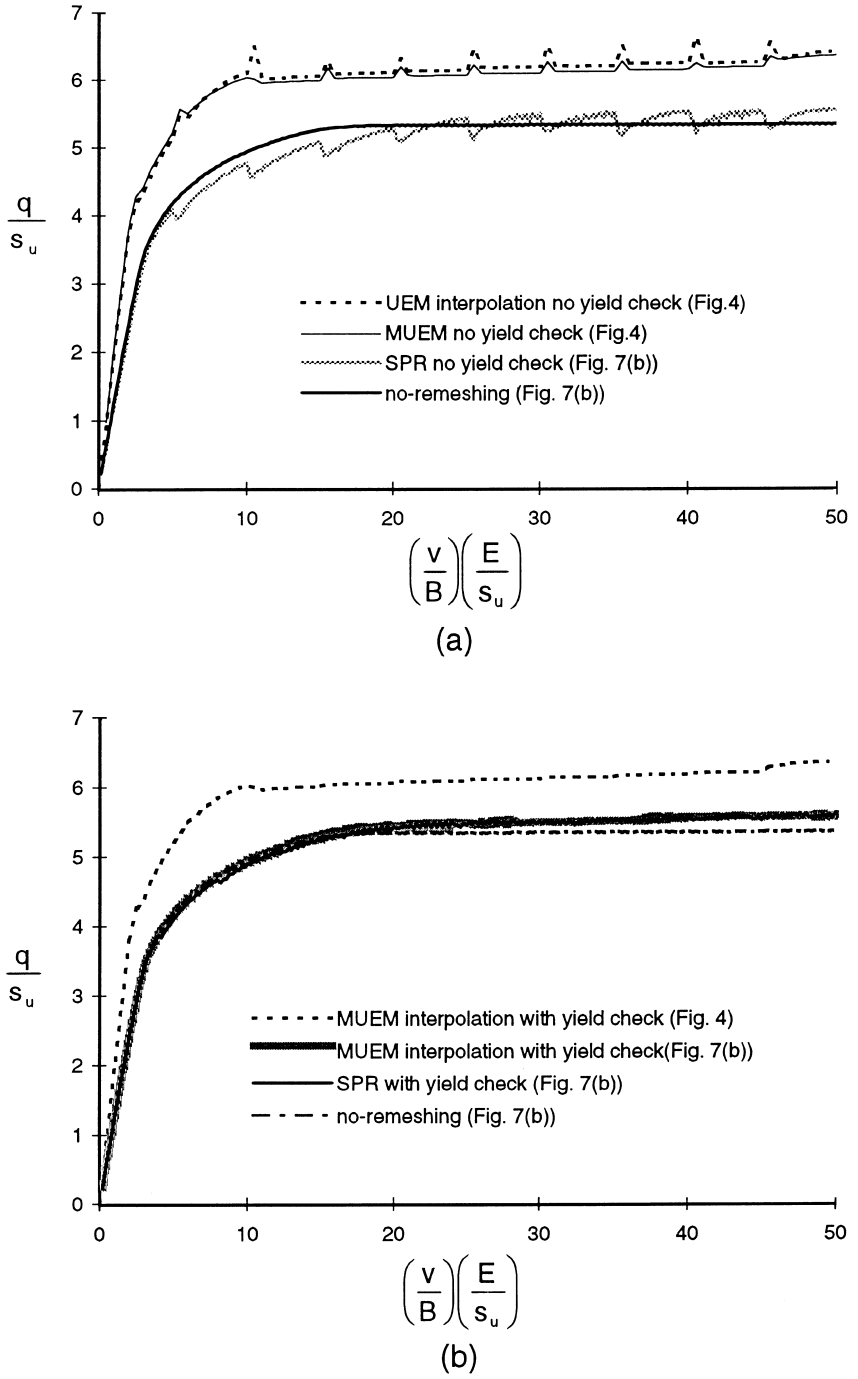


Fig. 5. Load–displacement response of strip foundation using MUEM and SPR for interpolation.

section "Refinement using subdivision concept", which leads to a mesh with least elements for a satisfactory FE result. Although this approach needs more cycles (three compared with the single step approach of the section "One-cycle mesh refinement"), it is only needed at the very start of a large deformation analysis, with any further mesh refinement occurring in one cycle during subsequent remeshing. This approach has therefore been adopted for the following analyses.

### 4.3. Strip foundation in non-homogeneous soil

The bearing capacity of a strip foundation on non-homogeneous soil is analysed for different values of $kB/s_{uo}$ (see Table 1). It was found that, for high degree of non-homogeneity, $kB/s_{uo} > 4$, the adaptive mesh using strain-SPR error criterion alone did not give satisfactory result, compared with analytical solutions. This is because the non-homogeneity of the soil is not considered in the *h*-adaptive mesh refinement, and for high non-homogeneity a restriction needs to be placed on the minimum size of element. Through numerical experiments, some criteria for element size and displacement increment size $\delta$ are proposed here, for six-noded elements:

$$\frac{h_{\min}}{B} = 0.01 \tag{18}$$

$$\frac{h_{uf}k}{s_{uo}} = 0.3 \tag{19}$$

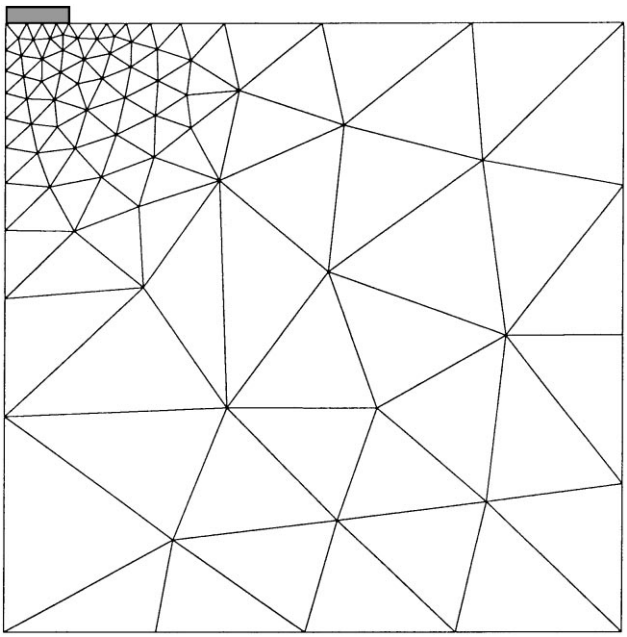

Fig. 6. Coarse starting mesh for adaptive refinement.

$$\left(\frac{\delta}{B}\right)\left(\frac{E}{s_u}\right)\left(\frac{kB}{s_{uo}}\right)^{0.8} = 0.17 \tag{20}$$

where $h_{uf}$ is the element size under the foundation. The criterion of Eq. (20) should only be applied in the final cycles of mesh refinement [having first satisfied Eq. (18)] in order to obtain a mesh with least elements. Fig. 8 shows the resulting mesh using these criteria for different ratio of $kB/s_{uo}$. It can be seen that the mesh under the footing is refined across the full width of the footing for high degree of non-homogeneous soil.

The computed load–displacement responses for soil with $kB/s_{uo} = 2$ to 30 are shown in Fig. 9. It may be seen from Fig. 9(a) that all the load–displacement curves have different starting gradients, which makes it difficult to control accuracy in the computation. However, Fig. 9(b) shows that the initial gradients may be brought

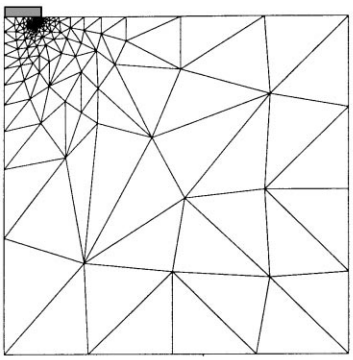

(a) One-cycle refinement (NUMEL=352)

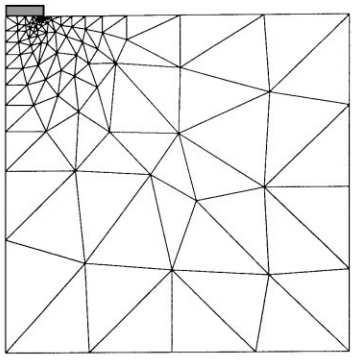

(b) Refinement with 4 cycles of subdivision (NUMEL=209)

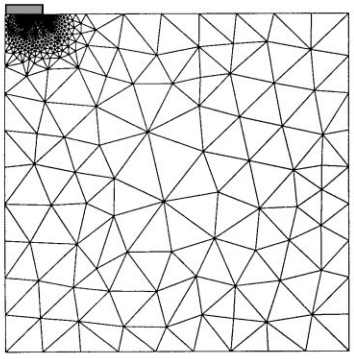

(c) Mesh density using exponential function (NUMEL=1166)

Fig. 7. Comparison of different mesh refinement.

Table 1
Bearing capacity for rough strip foundation

| | | FE initial mesh | FE adaptive mesh | Davis and Booker [17] | | Houlsby and Wroth [18] | | Tani and Craig [19] | |
|---|---|---|---|---|---|---|---|---|---|
| $kB/s_{uo}$ | $\delta/B$ [Eq. (20)] | $q_u/s_{uo}$ | $q_u/s_{uo}$ (reduction %) | $q_u/s_{uo}$ | Error (%) | $q_u/s_{uo}$ | Error (%) | $q_u/s_{uo}$ | Error (%) |
| 2 | 0.0002 | 9.14 | 7.94 (15.1) | 7.65 | 3.7 | 7.57 | 4.7 | 7.75 | 2.5 |
| 4 | 0.0001 | 11.62 | 9.67 (20.2) | 9.21 | 4.8 | 9.04 | 6.5 | 9.23 | 4.8 |
| 6 | 0.00008 | 13.85 | 11.03 (25.6) | 10.49 | 5.1 | 10.37 | 6.0 | 10.49 | 5.1 |
| 8 | 0.00006 | 15.95 | 12.32 (29.5) | 11.71 | 5.2 | 11.52 | 6.5 | — | — |
| 10 | 0.00005 | 18.01 | 13.51 (33.3) | 12.88 | 4.9 | 12.67 | 6.2 | 12.73 | 5.8 |
| 15 | 0.00003 | 23.11 | 16.20 (42.7) | 15.43 | 5.0 | — | — | — | — |
| 30 | 0.00002 | 37.95 | 23.06 (64.6) | 22.31 | 3.4 | — | — | 21.69 | 5.9 |

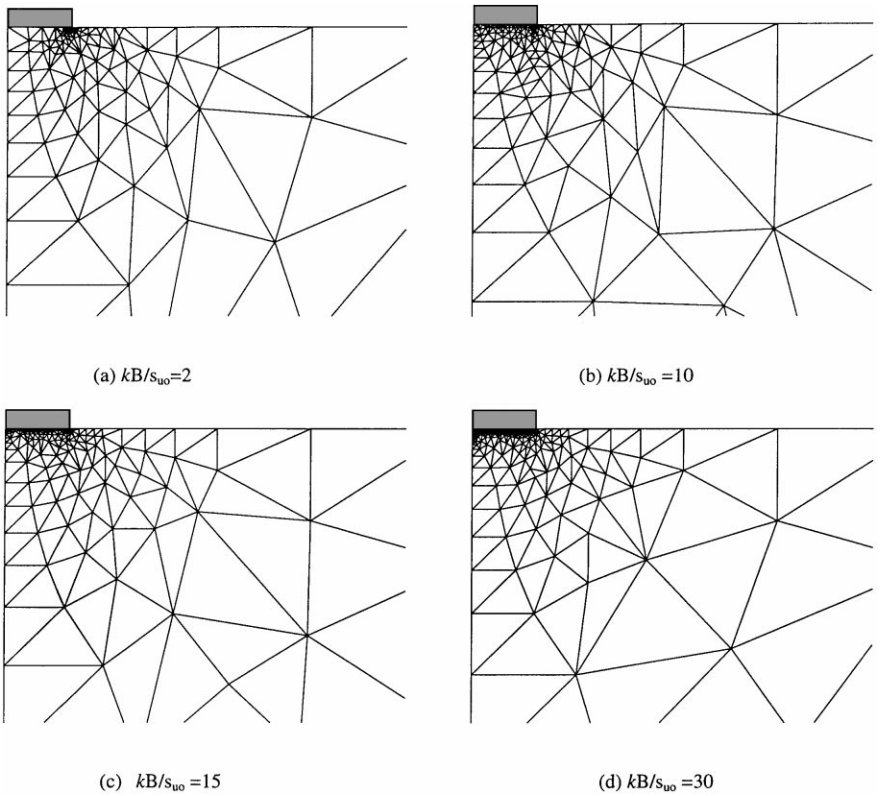


Fig. 8. Adaptive refined mesh in different ratio of $kB/s_{uo}$ for strip foundation analysis.

together using the alternative form of normalised displacement $(v/B) * (E/s_u) * (kB/s_{uo})^{0.8}$; this is the key to the use of Eq. (20) to control the displacement increment size for different values of $kB/s_{uo}$. The values of bearing capacity and errors, compared with published lower bound solutions, are listed in Table 1. Because the analytical solutions listed in Table 1 are stress characteristics (lower bound) solutions, the accuracy of the FE solution should be compared only with the largest bound solution in each case, which is generally that from Davis and Booker [17].

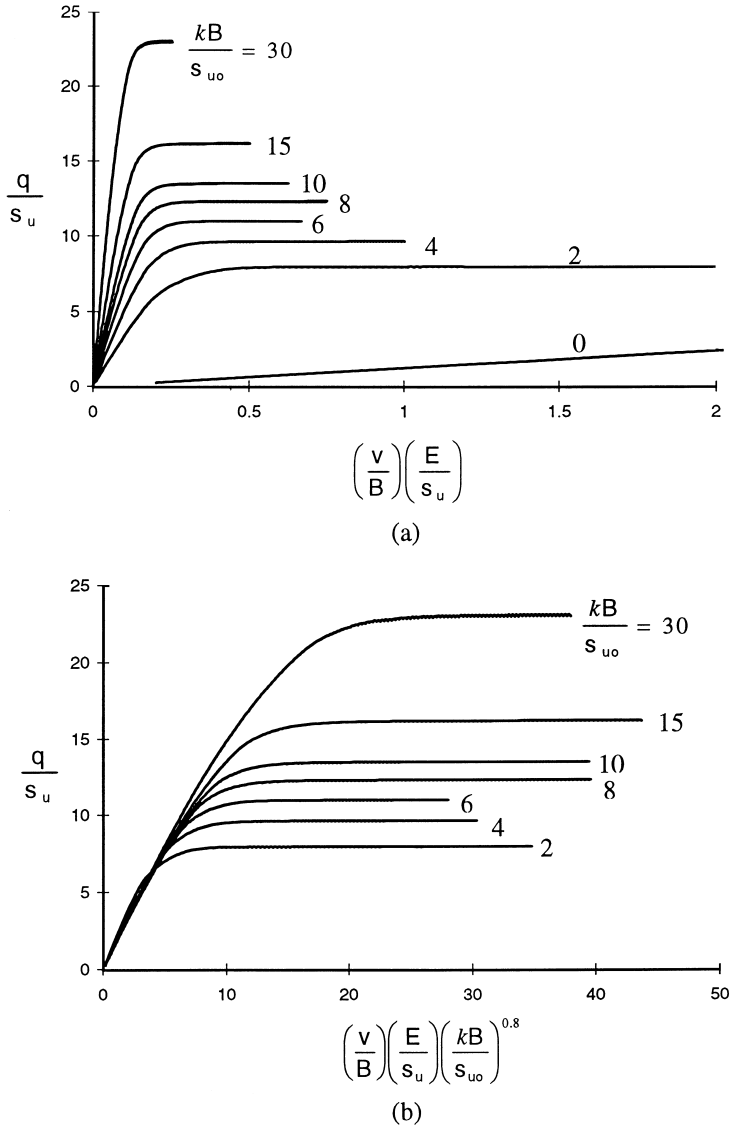


Fig. 9. Load–displacement response of strip foundations in non-homogeneous soil.

The FE results using the initial coarse mesh (Fig. 6) are also listed in the table to compare with the FE results using the refined adaptive mesh. It was found that a given mesh can give reasonable results for low degrees of non-homogeneity, but very inaccurate results for higher degrees of non-homogeneity. The FE results using the adaptive meshes are satisfactory (noting that the non-linear solution algorithm in AFENA is a simple tangent stiffness approach, with no iteration), with errors generally less than 5% of the analytical solutions. Therefore, Eqs. (18) to (20) offer a good guidance for practical computations.

### 4.4. H-*Adaptivity in large deformation analysis of strip foundation*

For large deformation analysis, *h*-adaptive mesh generation and remeshing has been implemented within RITSS. The numerical procedure is summarised below:

(a) "Element subdivision" refinement with a few cycles, with tolerance of $h_{\min}$ and $h_{1uf}$, at the start of the analysis to achieve the desired mesh;
(b) incremental small displacement analysis using AFENA [16];
(c) mesh regeneration (or remeshing) using updated soil boundary and element subdivision refinement, but with only one cycle;
(d) stress interpolation using MUEM (or SPR);
(e) repeat of steps (c) and (d) until the required total displacement is achieved.

A rough strip footing, with smooth vertical sides and penetrating from the soil surface, has been analysed for non-homogeneity of $kB/s_{uo} = 10$. The analysis starts from the adaptive mesh shown in Fig. 8(b), with displacement increment $\delta(v/B) = 0.00006$, and remeshing interval $\Delta(v/B) = 25 * \delta(v/B) = 0.0015$. Fig. 10 shows the resulting load-placement response, with and without soil weight of

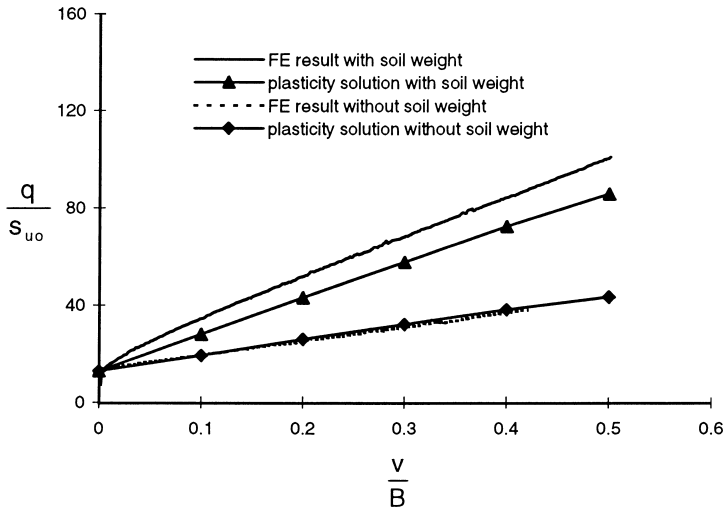


Fig. 10. Large deformation analysis of strip foundation for $kB/s_{uo} = 10$.

$\gamma/k = 8.5$. The FE results are compared with Davis and Booker's solutions [17], where allowance is made for increasing $s_{uo}$ (and thus decreasing $kB/s_{uo}$) as the foundation penetrates into the soil.

The FE results agree well with Davis and Booker's solution [17] at the start of penetration, allowing for the error of 5% noted earlier. In the analysis without soil weight, the numerical result falls marginally below the plasticity solution at deeper penetration. This is because the rough footing has trapped weak soil from the soil surface immediately below it, and this effect dominates over that of increasing penetration [2]. For the case with soil self-weight, as the penetration increases, the FE result rises significantly above the plasticity solution (by over 30%). This is because the soil heave on either side of the foundation makes an important contribution to the bearing capacity.

Fig. 11 shows the deformed soil shape with yielded zone and displacement vectors from the large deformation analysis with and without soil weight, when $v/B = 0.4$.

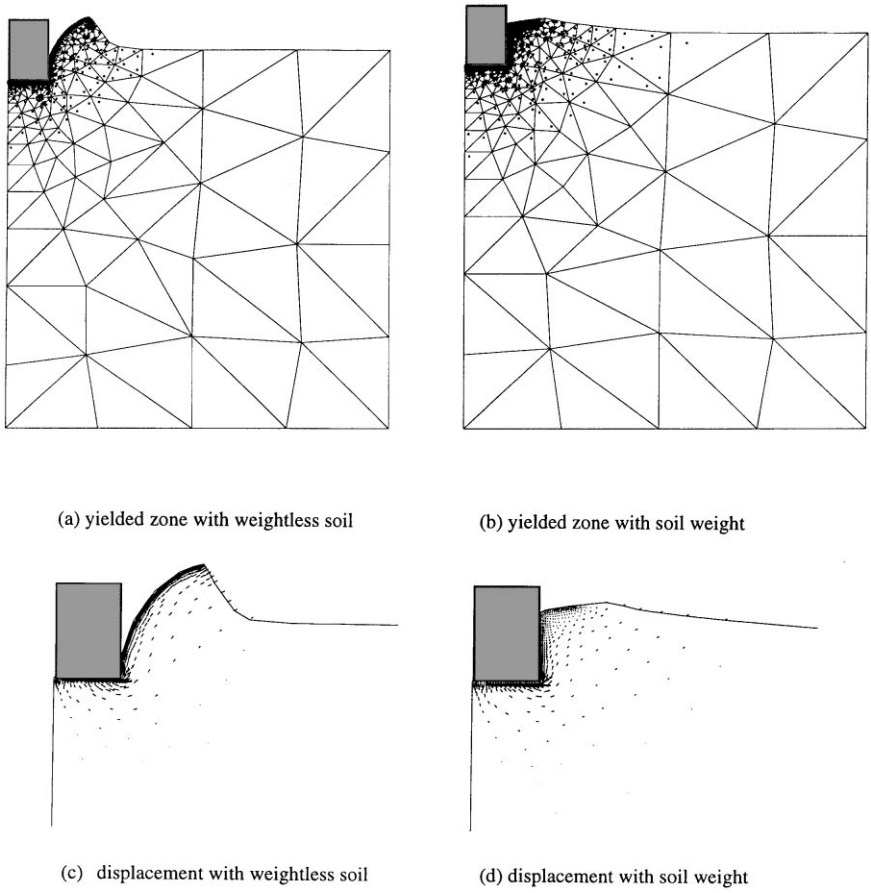


Fig. 11. Deformed soil in strip foundation analysis for $v/B = 0.4$, $kB/s_{uo} = 10$.

Clear differences may be seen in the surface profile of the soil, with the analysis allowing for soil weight showing a more realistic, flatter, surface, but still with significant heave adjacent to the foundation.

### 4.5. H-Adaptivity in bearing capacity analysis of circular foundation

Although strip foundations have advantages for evaluation of new numerical approaches, because of their simplicity and the availability of bound solutions, most actual foundations are closer to circular in plan. To illustrate practical application of $h$-refinement in mesh generation, the bearing capacity of a circular foundation on non-homogeneous soil has been studied for different degrees of soil non-homogeneity.

The initial mesh shown in Fig. 6 has been used, with radial and vertical boundaries of 10 times the foundation radius, $R$, or 5 times the diameter, $D$. The base of the foundation has been taken as fully rough, and the response has been analysed for soil with non-homogeneity degree ($kD/s_{uo}$) of up to 30.

The criteria proposed for size of element and displacement increment are:

$$\frac{h_{\min}}{D} = 0.005 \tag{21}$$

$$\frac{h_{uf}k}{s_{uo}} = 0.2 \tag{22}$$

$$\left(\frac{\delta}{D}\right)\left(\frac{E}{s_u}\right)\left(\frac{kD}{s_{uo}}\right)^{0.8} = 0.03 \tag{23}$$

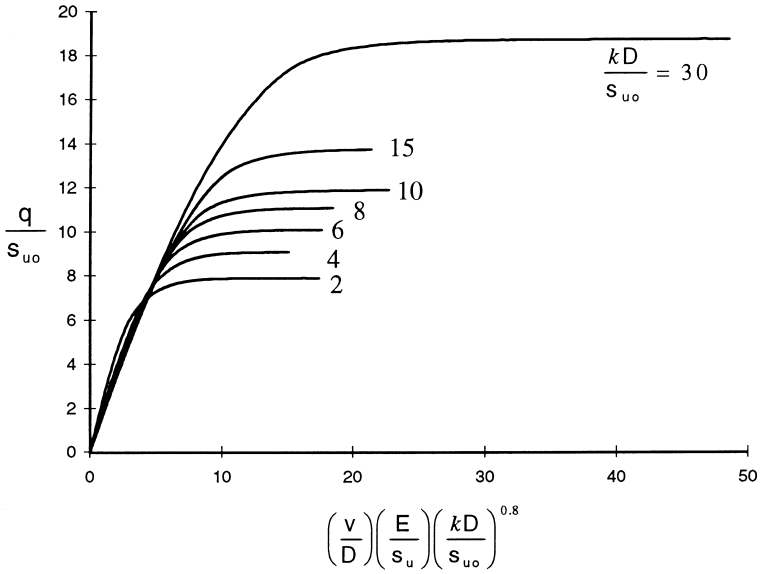


Fig. 12. Load–displacement response of circular foundations in non-homogeneous soil.

Table 2
Bearing capacity for rough circular foundation

| | | FE initial mesh | FE adaptive mesh | Houlsby and Wroth [18] | | Tani and Craig [19] | |
|---|---|---|---|---|---|---|---|
| $kD/s_{uo}$ | $\delta/D$ [Eq. (23)] | $q_u/s_{uo}$ | $q_u/s_{uo}$ (reduction %) | $q_u/s_{uo}$ | Error (%) | $q_u/s_{uo}$ | Error (%) |
| 2 | 0.00004 | 9.93 | 7.89 (25.8) | 7.61 | 3.5 | 7.70 | 2.5 |
| 4 | 0.00002 | 11.93 | 9.07 (31.5) | 8.71 | 4.0 | 8.77 | 3.4 |
| 6 | 0.000014 | 13.80 | 10.09 (36.8) | 9.67 | 4.2 | 9.72 | 3.8 |
| 8 | 0.000012 | 15.82 | 11.00 (43.8) | 10.54 | 5.1 | — | — |
| 10 | 0.00001 | 17.83 | 11.77 (51.5) | 11.33 | 3.7 | 11.38 | 3.4 |
| 15 | 0.000007 | 22.21 | 14.68 (51.3) | — | — | — | — |
| 30 | 0.000004 | 32.24 | 18.78 (71.7) | — | — | 18.07 | 3.9 |

Comparing Eqs. (18) to (20) with Eqs. (21) to (23), it can be seen that the minimum element size is approximately half that for the strip foundation analysis, while the displacement increment size is reduced by a factor of over 5. The higher mesh refinement is necessary owing to the limitations of the linear strain triangular element for axisymmetric analysis, although the use of only three Gauss points per element avoids actual locking [20]. Fifteen-noded triangular elements would be superior, although the number of degrees of freedom might need to be larger than for the six-noded elements, for high degrees of soil non-homogeneity. At present, the remeshing techniques have not been extended to the higher order elements, since the six-noded elements have been found to perform reasonably, provided the element size and displacement increment are small enough.

Fig. 12 shows the load-displacement response of a circular foundation on non-homogeneous soil, for small strain analysis without remeshing (apart from the adaptive mesh cycles at the start of the analysis). It is apparent that a true collapse load is obtained, with zero terminal gradient. Table 2 gives the numerical results compared with published lower bound solutions. The FE results using the initial coarse mesh (Fig. 6) are tabulated to compare with the FE results using the refined adaptive mesh. It is apparent that the accuracy of the FE result using the initial mesh decreases as the degree of non-homogeneity increases. The errors show the comparison between the FE results using the adaptive mesh with the published plasticity solutions. The relatively small errors justify the criteria given by Eqs. (21) to (23).

## 5. Concluding remarks

*H*-Adaptive mesh refinement, which reduces the element size without changing the order of the polynomial expansions, is simple to implement in an existing finite element codes. Although the adaptive mesh generation has been studied by many

researchers since the 1980s, it has mainly been tested for linear elastic problems. For non-linear elasto-plastic problems, a strain-SPR error measure is proposed in this paper, evaluated using superconvergent patch recovery (SPR), which gives a dramatic increase in the accuracy of strains and stresses from the finite element solution. The resulting *h*-adaptive mesh generation allows optimal meshes to be developed, using multiple-cycle element subdivision until a minimum element-size criterion is satisfied.

In large deformation analysis, using RITSS (small strain incremental analysis with periodic remeshing) [1], stress interpolation using either the modified unique element method (MUEM) or the SPR approach gives a smooth load-displacement response after each remeshing, but only provided the stress field is corrected to the yield envelope in regions of yield.

The approaches have been applied to the analysis of bearing capacity of strip and circular foundations on non-homogeneous soil, where the soil strength increases linearly with depth. Criteria for minimum element size and displacement increment have been proposed, allowing for the degree of soil non-homogeneity. It has been found that, to achieve a given accuracy, analysis of circular foundations needs finer mesh (minimum element size approximately half that for strip foundation) and displacement increments a factor of five smaller than for analysis of strip foundations. The proposed criteria provide a practical guide for accurate analysis, applicable to a simple tangent stiffness solution algorithm, without iteration.

For large deformation analysis, even though a few cycles of mesh refinement are needed to obtain an optimal mesh from the initial coarse mesh, this only needs to be done at the very start of the analysis. At each subsequent remeshing, a single cycle of refinement is adequate. The overall approach has been illustrated with large deformation analysis of a strip foundation penetrating into non-homogeneous soil by up to half the foundation width. The soil self-weight was shown to have a significant effect on the resulting pattern of heave adjacent to the foundation, and also on the relative magnitude of the bearing capacity, compared with lower bound solutions that ignore such heave.

## Acknowledgements

The work in this paper forms part of the Special Research Centre for Offshore Foundation Systems, established and supported under the Australia Research Council's Research Centres Program. This support is gratefully acknowledged.

## References

[1] Hu Y, Randolph MF. A practical numerical approach for large deformation problems in soil. Int. Journal of Numer. Analyt. Methods Geo., 1998;22:327–50.

[2] Hu Y, Randolph, MF. A fully automatic mesh generation method for large deformation problem of soil. Eighth Int. Conference of Computer Methods and Advances in Geomechanics, 1994;1:441–6.

[3] Hu Y, Randolph MF. Numerical simulation of pipe penetration in non-homogeneous soil. Proc. of 5th Int. Offshore and Polar Eng. Conf., 522–6.

[4] Hu Y, Randolph MF. Deep penetration of shallow foundations on non-homogeneous soil. Soils and Foundations 1998;38(1):241–6.
[5] Zienkiewiecz OC, Zhu JZ. Adaptivity and mesh generation. Int. Journal of Numer. Methods Eng. 1991;32:783–810.
[6] Belytschko T, Tabbara M. H-adaptivity finite element methods for dynamic problems, with emphasis on localization. Int. Journal of Numer. Methods Eng. 1993;36:4245–65.
[7] Zienkiewiecz OC, Zhu JZ. A simple error estimator and adaptive procedure for practical engineering analysis. Int Journal of Numer Methods Eng 1987;24:337–57.
[8] Babuska I, Rheinboldt HJ. Error estimates for adaptive finite element computations. SIAM Journal of Numer. Anal. 1978;15(4):736–54.
[9] Diaz AR, Kikuchi P, Taylor JE. Design of an optimal grid for finite element methods. Journal of Struct. Mech. 1983;11:215–30.
[10] Oden JT, Brauchli HJ. On the calculation of consistent stress distributions in finite element applications. Int Journal of Numer Methods Eng 1971;3:317–25.
[11] Zienkiewiecz OC, Zhu JZ. The superconvergent patch recovery and a posteriori error estimates. Part 1: The recovery technique. Int. Journal of Numer. Methods Eng. 1993;33:1331–1364.
[12] Zienkiewicz OC, Zhu JZ, Wu J. Superconvergent patch recovery techniques—some further tests. Communications Numer. Methods Eng. 1993;9:251–8.
[13] Zienkiewicz OC, Huang M, Pastor M. Localization problems in plasticity using finite elements with adaptive remeshing. Numer Analyt Methods Geo 1995;19(2):127–148.
[14] Wiberg NE, Li XD, Abdulwahab F. Adaptive finite element procedures in elasticity and plasticity. Eng Comp 1996;12:120–141.
[15] Mucke P, Whiteman JR. A posteriori error estimates and adaptivity for finite element solutions in finite elasticity. Int Journal of Numer Methods Eng 1995;38:775–95.
[16] Carter, J. P. and Balaam, N., AFENA Users Manual. Geotechnical Research Centre, The University of Sydney, 1990.
[17] Davis EH, Booker JR. The effect of increasing strength with depth on the bearing capacity of clays. Geotechnique 1973;23(4):551–63.
[18] Houlsby GT, Wroth CP. Direct solution of plasticity problems in soils by the method of characteristics. Proc. 4th ICONMIG 1982;3:1059–1071.
[19] Tani K, Craig WH. Bearing capacity of circular foundations on soft clay of strength increasing with depth. Soils and Foundations 1995;35(4):21–35.
[20] Sloan SW, Randolph MF. Numerical prediction of collapse loads using finite element methods. Int. Journal of Numerical and Analytical Methods in Geomechanics 1985;6:47–76.